Syntheses and Self-Assembly of Poly(benzyl ether)-*b*-Poly(*N*-isopropylacrylamide) Dendritic–Linear Diblock Copolymers

ZHISHEN GE,[1] SHIZHONG LUO,[2] SHIYONG LIU[1,2]

[1]Department of Polymer Science and Engineering, University of Science and Technology of China, Hefei, Anhui, China

[2]Laboratory of Macromolecular Colloids and Solutions, Hefei National Laboratory for Physical Sciences at Microscale, Hefei, Anhui, China

Received 13 September 2005; accepted 25 November 2005
DOI: 10.1002/pola.21261
Published online in Wiley InterScience (www.interscience.wiley.com).

ABSTRACT: This article describes the syntheses and solution behavior of model amphiphilic dendritic–linear diblock copolymers that self-assemble in aqueous solutions into micelles with thermoresponsive shells. The investigated materials are constructed of poly(benzyl ether) monodendrons of the second generation ([G-2]) or third generation ([G-3]) and linear poly(*N*-isopropylacrylamide) (PNIPAM). [G-2]-PNIPAM and [G-3]-PNIPAM dendritic–linear diblock copolymers have been prepared by reversible addition–fragmentation transfer (RAFT) polymerizations of *N*-isopropylacrylamide with a [G-2]- or [G-3]-based RAFT agent, respectively. The critical micelle concentration (cmc) of [G-3]-$PNIPAM_{220}$, determined by surface tensiometry, is 6.3×10^{-6} g/mL, whereas [G-2]-$PNIPAM_{235}$ has a cmc of 1.0×10^{-5} g/mL. Transmission electron microscopy results indicate the presence of spherical micelles in aqueous solutions. The thermoresponsive conformational changes of PNIPAM chains located at the shell of the dendritic–linear diblock copolymer micelles have been thoroughly investigated with a combination of dynamic and static laser light scattering and excimer fluorescence. The thermoresponsive collapse of the PNIPAM shell is a two-stage process; the first one occurs gradually in the temperature range of 20–29 °C, which is much lower than the lower critical solution temperature of linear PNIPAM homopolymer, followed by the second process, in which the main collapse of PNIPAM chains takes place in the narrow temperature range of 29–31 °C. J Polym Sci Part A: Polym Chem 44: 1357–1371, 2006
Keywords: dendrimers; diblock copolymers; self-assembly; reversible addition fragmentation chain transfer (RAFT)

INTRODUCTION

Dendrimers with well-defined architectures are considered promising candidates for functional supramolecular materials.[1–3] Dendrimers can be made amphiphilic through the modification of the nature and size of the functional end groups, fragments, and building blocks.[4–7] Dendritic amphiphiles can be considered unimolecular micelles. They possess unique features that distinguish them from block copolymer micelles, in that they have a well-defined branched structure that emanates from a central core and a highly organized interior.[8–10] They could potentially serve as nano-

Correspondence to: S. Liu (E-mail: sliu@ustc.edu.cn)
Journal of Polymer Science: Part A: Polymer Chemistry, Vol. 44, 1357–1371 (2006)

containers for the entrapment of guest molecules.[3] Unfortunately, only a few guest molecules of relatively small size can be encapsulated even in higher generation dendritic molecules; this is due to the fact that the dendrimer interior has a semirigid molecular construction with a prearranged geometry and dimensions of interior cavities.[11(a)] Thus, amphiphilic dendritic–linear block copolymers are believed to combine the advantageous properties of both linear and dendritic amphiphiles.[12–16] Using dendritic blocks as the core-forming components and flexible chains for the coronal loops is especially attractive because it can provide an easy approach for the construction of a nonentangled and highly ordered entity in the center of the aggregates. Thus, the micellar core will be capable of accommodating a large number of guest molecules not only in the internal voids of the dendrons but also in the void spaces between individual monodendrons.

Dendritic–linear diblock copolymers have been synthesized with a variety of different synthetic strategies.[11(b)] The first strategy involves the coupling of preformed linear polymers functionalized at one or both chain ends with reactive dendrons having a complementary functionality at their focal point.[11,17–19] Meijer, Chapman, and coworkers[20–22] have demonstrated an alternative approach, in which the dendritic segment is grown via a divergent strategy from a suitably end-functionalized linear polymer. Reactive dendrons can also serve as macromolecular initiators in the anionic polymerization of ε-caprolactone[23] and living/controlled free-radical polymerization of vinyl monomers.[15,16] Poly(benzyl ether) dendrons containing either a single benzylic (2,2,6,6-tetramethylpiperidinyl-1-oxy) (TEMPO) or halide functionality at their focal point have been used for the nitroxide-mediated polymerization and atom transfer radical polymerization (ATRP) of styrene, *t*-butyl acrylate, and *N*-isopropylacrylamide (NIPAM) to synthesize dendritic–linear diblock copolymers.[15,16,24] Reversible addition–fragmentation transfer (RAFT) has recently emerged as a promising controlled free-radical polymerization technique because of its versatility and simplicity, and the polymer is free from the contamination of metal catalysts.[25–27] Most importantly, it is compatible with almost all conventional free-radical polymerization monomers.

The interest in stimuli-responsive polymers has exponentially increased because of their promising potential in a variety of applications for biomedical fields.[28–34] Among them, temperature- and pH-responsive mechanisms have been extensively investigated because they are relatively convenient and effective stimuli in many applications. The reports of stimuli-responsive dendritic–linear diblock copolymers are still rare. Fréchet et al.[13] synthesized dendritic–linear diblock copolymers comprising poly(ethylene oxide) and water-soluble polylysine dendrons; hydrophobic groups were attached to the dendrimer periphery by highly acid-sensitive cyclic acetals to render the water-soluble polylysine dendrimer hydrophobic. This interesting dendritic–linear diblock copolymer forms stable micelles in aqueous solutions at a neutral pH but disintegrates into unimers at a mildly acidic pH after the loss of hydrophobic groups upon acetal hydrolysis. Zhu and coworkers[24] synthesized a poly(benzyl ether)–poly(acrylic acid) amphiphilic dendritic–linear block copolymer by the hydrolysis of a poly(benzyl ether)–poly(*t*-butyl acrylate) dendritic–linear diblock copolymer, which was synthesized by the ATRP of *t*-butyl acrylate with a poly(benzyl ether) dendrimer with a benzyl bromide group at the focal point as the initiator.

Poly(*N*-isopropylacrylamide) (PNIPAM) undergoes a phase transition at its lower critical solution temperature (LCST) of 32 °C, and it has been widely studied as a polymer potentially useful for targeted drug delivery.[35] Zhu and coworkers[24] synthesized a poly(benzyl ether)–poly(*N*-isopropylacrylamide) dendritic–linear diblock copolymer via the ATRP technique with second-generation dendritic poly(benzyl ether) bromide ([G-2]-CH_2Br) as the initiator. Conventional catalyst systems of ATRP processes such as CuBr/2,2′-bipyridine cannot polymerize NIPAM; in the studies by Zhu and coworkers,[24] CuBr/1,4,8,11-tetramethyl-1,4,8,11-tetraazacyclotetradecane catalysts were used to polymerize NIPAM, but they did not give the polymerization kinetics. [G-2]-poly(*N*-isopropylacrylamide) ([G-2-PNIPAM) form micelles in aqueous solution, which is reported to have a phase-transition temperature of 37.5 °C. Because PNIPAM chains were linked to a hydrophobic core, the reported value is unreasonable as it is well known that the LCST of PNIPAM will decrease when it is randomly copolymerized or block-copolymerized with a hydrophobic monomer.[35]

Recent progress in living/controlled free-radical polymerization has shown that NIPAM can be controllably polymerized by the RAFT technique.[36–40] Here we synthesized poly(benzyl ether)–poly(*N*-isopropylacrylamide) dendritic–linear diblock copolymers by RAFT polymerization with a RAFT agent based on a second- or third-generation poly(benzyl ether) dendrimer ([G-2] or [G-3],

respectively); the polymerization kinetics were investigated in detail. To the best of our knowledge, this is the first report of the syntheses of dendritic–linear diblock copolymers employing the RAFT technique. The thermoresponsive conformational changes of PNIPAM chains located at the shell of the dendritic–linear diblock copolymer micelles have been thoroughly investigated with a combination of dynamic and static laser light scattering (LLS) and excimer fluorescence measurements.

EXPERIMENTAL

Materials

[G-2]-CH_2Br and the third-generation dendritic poly(benzyl ether) bromide ([G-3]-CH_2Br) used throughout this study were synthesized according to literature procedures.[41] NIPAM (97%; Tokyo Kasei Kagyo Co.) was purified by recrystallization in a benzene/*n*-hexane mixture. 2,2′-Azobis(isobutyronitrile) (AIBN) was recrystallized from ethanol. Petroleum ether, *n*-hexane, tetrahydrofuran (THF), 1,4-dioxane, and *N*,*N*-dimethylformamide (DMF) were dried over calcium hydride and distilled just before use.

Sample Preparation

Typical Synthesis of the [G-3]-Based RAFT Agent

Phenylmagnesium bromide was prepared from bromobenzene (0.785 g, 5 mmol) and magnesium turnings (0.125 g, 5.25 mmol) in dry THF. The solution was heated to 40 °C, and carbon disulfide (0.3625 g, 5 mmol) was then added dropwise over approximately 15 min to produce a dark brown solution. [G-3]-CH_2Br (3.31 g, 2 mmol) was added to the solution. The temperature was raised to 80 °C and maintained for 24 h. Ice-cooled water was then added to the solution, and the organic products were extracted with dichloromethane three times. The combined organic extracts were rinsed with water and dried over anhydrous magnesium sulfate. After solvent removal, the mixture was subjected to column chromatography to obtain purified [G-3]-CH_2SSCPh, the [G-3]-based RAFT agent, as a red solid. The overall yield was 48.3%.

^1H NMR (300 MHz, $CDCl_3$, δ): 4.65 ([G-3]-CH_2SSCPh), 4.8–5.1 (Ar—CH_2—O), 6.43–6.85 (Ar*H*), 7.10–7.45 (Ph*H*), 7.9–8.03 (—SSCPh*H*).

The [G-2]-based RAFT agent was synthesized with similar procedures, as described previously.

Synthesis of [G-3]-PNIPAM

A general procedure for synthesizing [G-3]-PNIPAM was as follows. A glass ampule was charged with the [G-3]-based RAFT agent (0.173 g, 0.1 mmol), AIBN (2.05 mg, 0.0125 mmol), and NIPAM (3.39 g, 30 mmol) in 1,4-dioxane (4 mL); it was then degassed by three freeze–thaw cycles and sealed *in vacuo*. The polymerization was carried out at 80 °C for 12 h. The mixture was precipitated into anhydrous diethyl ether twice. The product was collected by filtration and then dried in a vacuum oven at room temperature. A pink-red solid was obtained. The degree of polymerization (DP) of the PNIPAM block was determined to be 220 by ^1H NMR.

[G-2]-PNIPAM was prepared with similar procedures, ^1H NMR analysis revealed a DP of 235 for the PNIPAM block. The molecular weight distributions of [G-2]-PNIPAM and [G-3]-PNIPAM were further analyzed by gel permeation chromatography (GPC).

Synthesis of [4-(1-Pyrenyl)butyl]acrylate (PyBA)

Acryloyl chloride (1.0 mL, 12.3 mmol) was added to a stirred solution of 1-pyrene butanol (1.0 g, 3.6 mmol) and triethylamine (1.5 g, 15 mmol) in 20 mL of dichloromethane over a period of 1 h under nitrogen at 0 °C. The reaction mixture was stirred overnight at room temperature in the dark; it was diluted with chloroform (50 mL) and filtered to remove triethylamine hydrochloride that formed during the reaction. The filtrate was washed with 1 M HCl, brine, 1 M $NaHCO_3$, and brine successively. The organic layer was dried over anhydrous magnesium sulfate, filtered, and evaporated under reduced pressure to give a yellow product.

Synthesis of Pyrene-Labeled [G-3]-PNIPAM

The general procedure for synthesizing [G-3]-PNIPAM was as follows. A glass ampule was charged with the [G-3]-based RAFT agent (0.173 g, 0.1 mmol), AIBN (2.05 mg, 0.0125 mmol), NIPAM (3.45 g, 35 mmol), and PyBA (0.1148 g, 0.35 mmol) in 1,4-dioxane (4 mL); it was then degassed by three freeze–thaw cycles and sealed *in vacuo*. The polymerization was carried out at 80 °C for 12 h. The mixture was precipitated into anhydrous diethyl ether twice. The product, [G-3]-PNIPAM-Py, was collected by filtration and then dried in a vacuum oven at room temperature. A pink-red solid was obtained.

General Procedures for the Preparation of Micelles

[G-2]-PNIPAM$_{235}$ and [G-3]-PNIPAM$_{220}$ are not directly soluble in water. Therefore, during the preparation of the micelles, a cosolvent approach was used. [G-2]-PNIPAM$_{235}$ or [G-3]-PNIPAM$_{220}$ was dissolved in DMF at a concentration of 1.0 g/L. Under vigorous stirring, water was added dropwise at a speed of 0.2 mL/min. The final water/DMF ratio in the mixed solution was 9/1 (v/v). After stirring for a further 10 h, DMF was thoroughly removed by dialysis against deionized water for 3 days. Fresh deionized water was replaced every 6 h. No residual DMF was detected in the final aqueous micellar solution, as determined by ^{1}H NMR.

Characterization

NMR Spectroscopy

All ^{1}H NMR spectra were recorded with a Bruker 300-MHz spectrometer. [G-3]-CH_2Br, the [G-3]-based RAFT agent, and [G-3]-PNIPAM were analyzed in $CDCl_3$.

GPC

The molecular weights and molecular weight distributions were determined by GPC with a series of two linear Styragel columns (HT3 and HT4) at an oven temperature of 60 °C. A Waters 1515 pump and a Waters 2414 differential refractive-index detector (set at 30 °C) were used. The eluent was DMF and 1 g/L LiBr at a flow rate of 1.0 mL/min. A series of six polystyrene standards with molecular weights ranging from 800 to 400,000 g/mol were used for calibration.

LLS

A commercial spectrometer (ALV/DLS/SLS-5022F) equipped with a multi-tau digital time correlation (ALV5000) and a Uniphase cylindrical, 22-mW He–Ne laser [wavelength of the laser light *in vacuo* (λ_0) = 632 nm] as the light source was used. In static LLS, we can obtain the weight-average molar mass (M_w) and the z-average root-mean square radius of gyration ($\langle R_g^2 \rangle^{1/2}$ or $\langle R_g \rangle$) of polymer chains in a dilute solution from the angular dependence of the excess absolute scattering intensity, known as the Rayleigh ratio [$R_{vv}(q)$], as follows:

$$\frac{KC}{R_{vv(q)}} \approx \frac{1}{M_w}\left(1 + \frac{1}{3}\langle R_g^2 \rangle q^2\right) + 2A_2C \qquad (1)$$

where K is equal to $4\pi n^2(dn/dC)^2/(N_A\lambda_0^4)$, C is polymer concentration, and q is equal to $(4\pi n/\lambda_0)\sin(\theta/2)$ with N_A, dn/dC, and n being the Avogadro number, the specific refractive-index increment, and the solvent refractive index, respectively, and A_2 is the second virial coefficient. dn/dC was determined by a precise differential refractometer at the same wavelength of 632 nm used in LLS measurements. In strict terms, $R_{vv}(q)$ should be $R_{vu}(q)$ because there was no analyzer before the detector. However, the depolarized scattering of the solution studied was insignificant, so $R_{vu}(q) \sim R_{vv}(q)$. Moreover, in this study, the sample solution was so dilute that the extrapolation of $C \to 0$ was not necessary, and the term $2A_2C$ in eq 1 could be neglected.

In dynamic LLS, the Laplace inversion of each measured intensity–intensity–time correlation function [$G^{(2)}(q,t)$] in the self-beating mode can lead to a line width distribution [$G(\Gamma)$]. For a pure diffusive relaxation, Γ is related to the translational diffusion coefficient (D) by $(\Gamma/q^2)_{C\to 0,q\to 0} \to D$ or further to the hydrodynamic radius (R_h) via the Stokes–Einstein equation, $R_h = (k_BT/6\pi\eta_0)/D$, where k_B, T, and η_0 are the Boltzmann constant, the absolute temperature, and the solvent viscosity, respectively.

Ultraviolet–visible (UV–vis) Spectroscopy and Transmittance Measurements

The UV–vis spectra and transmittance were acquired on a Unico UV–vis 2802PCS spectrophotometer. The transmittance of the solution was measured at a wavelength of 500 nm with a thermostatically controlled cuvette. The pyrene content in [G-3]-PNIPAM-Py was determined by UV–vis absorption in THF with 1-pyrenebutanol as a model compound.

Fluorescence Measurements

Fluorescence spectra were recorded with a Jasco FP-6200 spectrofluorometer. The temperature of the water-jacketed cell holder was controlled by a programmable circulation bath. The slit widths were set at 5.0 nm for both the excitation and emission. In a 1-cm cell, the samples were heated slowly at the heating rate of 0.1 °C/min. The excimer-to-monomer ratio was calculated as the ratio of the emission intensity at 480 nm to that of the emission at 373 nm.

The critical micelle concentration (cmc) was determined by a fluorescence technique. A calculated volume of the pyrene solution in acetone was added to a series of volumetric flasks, acetone

was removed under reduced pressure, polymer solutions at different concentrations were then added to the volumetric flasks, and the pyrene concentration was fixed at 5×10^{-7} mol/L. All the samples were sonicated for 2 h and then allowed to stand for 1 day before fluorescence measurements.

Transmission Electron Microscopy (TEM)

TEM observations were conducted on a Philips CM 120 electron microscope at an acceleration voltage of 100 kV. The sample for TEM observations was prepared by the placement of a 10-μL micellar solution at a concentration of 1.0×10^{-4} g/mL on copper grids coated with thin films of Formvar and carbon successively. No staining was required.

Surface Tensiometry

Equilibrium surface tensions were measured with a JK99B tensiometer with a platinum plate. The measuring accuracy of the device as reported by the manufacturer was ± 0.1 mN/m. The surface tension of pure water (ca. 71 mN/m) was checked periodically between measurements. The reported surface tension at each concentration was the average of three to five measurements that were taken after each of the solutions was allowed to equilibrate in the instrument at a temperature of $20.0 \pm 0.1\ ^{\circ}$C.

RESULTS AND DISCUSSION

Synthesis of the [G-3]-Based RAFT Agent, [G-3]-PNIPAM, and Pyrene-Labeled [G-3]-PNIPAM-Py

[G-3]-CH_2Br can be used as an ATRP initiator to polymerize conventional vinyl monomers such as styrene and alkyl (meth)acrylates.[15,16,24] However, there are several difficulties in polymerizing NIPAM with ATRP because of the interaction between NIPAM and Cu(I) complexes. Therefore, we have modified [G-3]-CH_2Br into a RAFT agent to mediate the polymerization of NIPAM.[24–27] A typical synthetic approach is shown in Scheme 1.

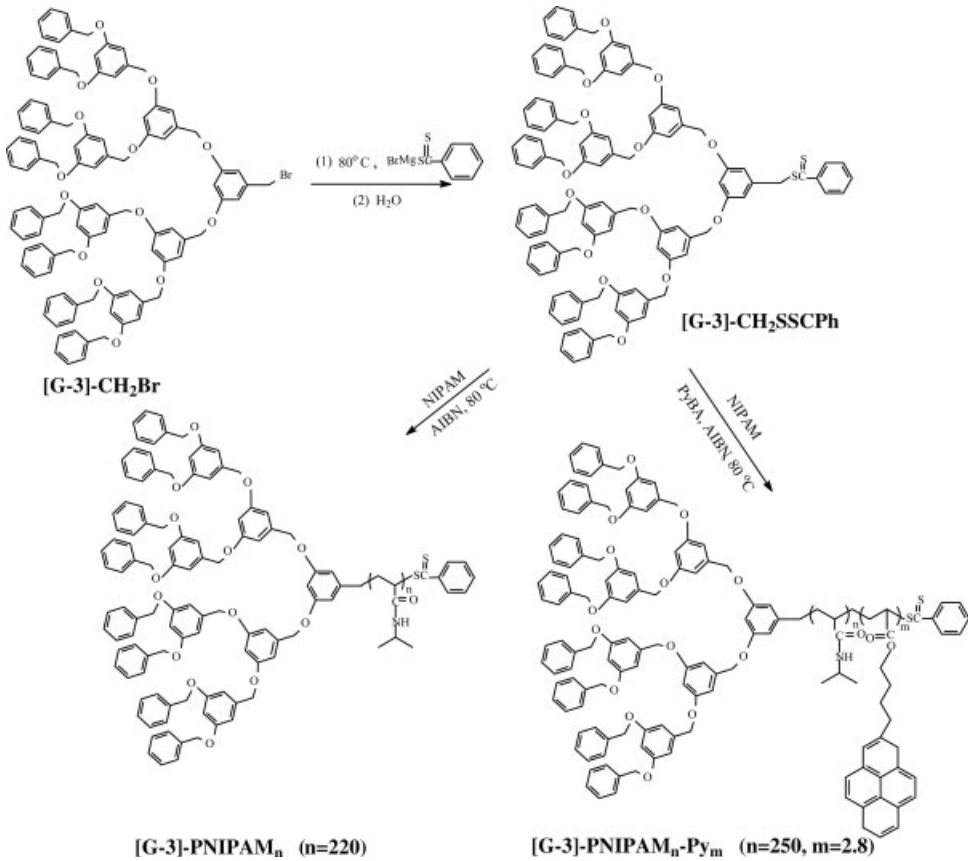

Scheme 1. Schematic illustration of the syntheses of [G-3]-$PNIPAM_{220}$ and [G-3]-$PNIPAM_{250}$-$Py_{2.8}$.

Synthesis of the [G-3]-Based RAFT Agent

The synthesis of the [G-3]-based RAFT agent was achieved through the addition of [G-3]-CH_2Br to a solution mixture of phenylmagnesium bromide and carbon disulfide in THF. To ensure the complete transformation of [G-3]-CH_2Br into the [G-3]-based RAFT agent, excess magnesium salt of dithiobenzoic acid was used. Column chromatography was necessary to obtain the pure [G-3]-based RAFT agent. Figure 1(a) shows the ^{1}H NMR spectrum of [G-3]-CH_2Br. The resonances for the exterior phenyl groups occur at 7.20–7.45 ppm, the resonances for the aromatics protons of the monomer units occur in the region of 6.50–6.70 ppm, and separate resonances can be observed in the appropriate ratio for each layer of monomer units. Resonances for the methylene protons of each monomer unit occur in the region of 4.80–5.10 ppm. The methylene resonances of —CH_2Br at the focal point can be seen at 4.40 ppm. In comparison with the ^{1}H NMR spectrum of the [G-3]-based RAFT agent shown in Figure 1(b), the resonances at 4.40 ppm have completely disappeared, and a new signal at $\delta = 4.60$ ppm has appeared. This indicates the complete transformation of [G-3]-CH_2Br into the RAFT agent [G-3]-CH_2SSCPh. We can also observe the appearance of signals at $\delta = 7.9$, 7.6 ppm, which have been ascribed to ortho and para protons of the dithiobenzoyl groups.

Synthesis of [G-3]-PNIPAM and Pyrene-Labeled [G-3]-PNIPAM-Py

Among various living radical polymerization techniques, the RAFT technique is now the best in controlling the molecular weight and molecular weight distribution of polyacrylamides. Rizzardo et al.[36] recently reported the synthesis of PNIPAM with a controlled molecular weight by RAFT polymerization with AIBN as an initiator and benzyl dithiobenzoate or cumyl dithiobenzoate as a RAFT agent. Müller et al.[37] reported the RAFT polymerization of NIPAM with benzyl 1-pyrrolecarbodithioate and cumyl 1-pyrrolecarbodithioate as RAFT agents in 1,4-dioxane at 60 °C. Here we used the [G-3]-based RAFT agent to polymerize NIPAM.

To verify that the growth of the NIPAM block via RAFT polymerization was conducted in a controlled manner, the polymerization process was monitored via sampling at different times for ^{1}H NMR and GPC analysis to determine the monomer conversion, molecular weight, and their distributions. Figure 2(a) shows the pseudo-first-order kinetic plot of the polymerization of NIPAM in the presence of the [G-3]-based RAFT agent. The linear plot of $\ln([M_0]/[M_t])$ versus the polymerization time until 80% conversion indicates that the concentration of chain radicals is constant during the polymerization, where $[M_0]$ and $[M_t]$ are monomer concentrations at time zero and t, respectively. The straight line almost passes through the origin, indicating that the RAFT polymerization of NIPAM with the [G-3]-based RAFT agent does not exhibit an induction period. The conversion continues to increase with the polymerization time and reaches about 80% after 12 h. The number-average molecular weight (M_n) increases almost linearly with the conversion, the and molecular weight distributions (M_w/M_n) remain relatively narrow (<1.3) throughout the polymerization process [Fig. 2(b)]. The obtained results are consistent with a controlled living free-radical polymerization process. Thus, we can facilely control the chain length and chain length distribution of the PNIPAM block with the [G-3]-based RAFT agent; this novel approach for preparing a [G-3]-PNIPAM dendritic–linear diblock copolymer is very convenient.

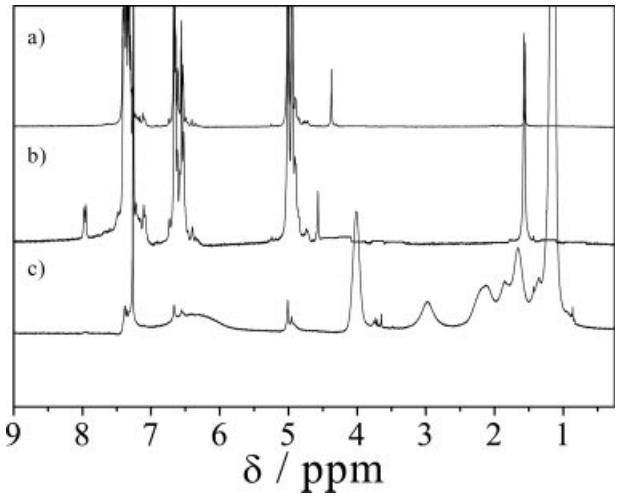

Figure 1. ^{1}H NMR spectra of (a) [G-3]-CH_2Br, (b) [G-3]-based RAFT agent [G-3]-CH_2SSCPh, and (c) dendritic–linear diblock copolymer [G-3]-$PNIPAM_{220}$.

Because the dendritic poly(benzyl ether) segments are insoluble in water, longer chains were designed to obtain stable micelles. The DPs of the PNIPAM block of [G-3]-PNIPAM and [G-3]-PNIPAM-Py were determined to be 220 and 250 by ^{1}H NMR. We denote them [G-3]-$PNIPAM_{220}$ and [G-3]-$PNIPAM_{250}$-Py, respectively. GPC traces in Figure 3 clearly show that the elution peak shifts to a higher molecular weight after the RAFT poly-

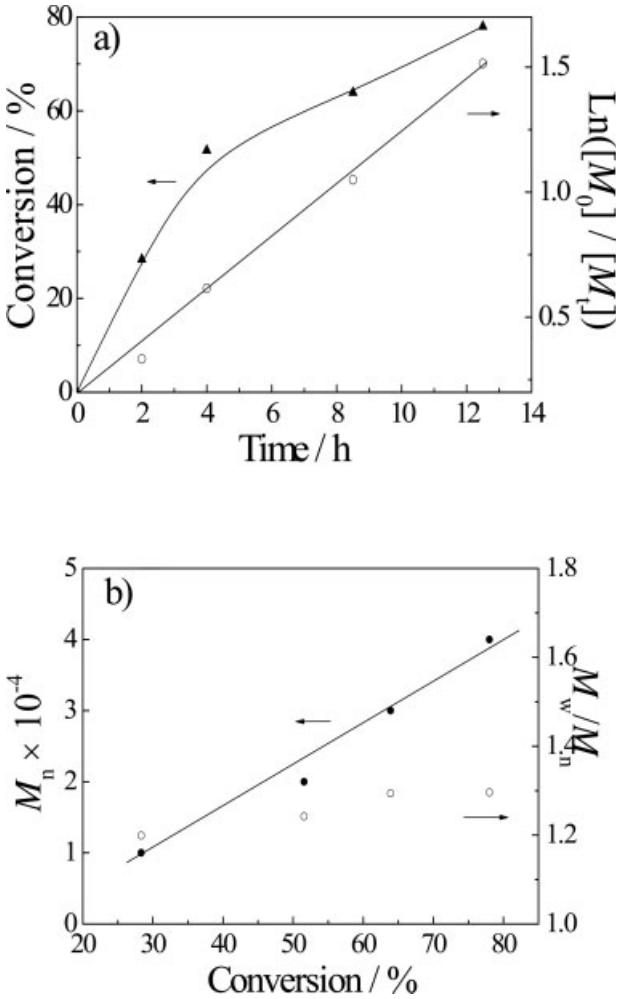

Figure 2. (a) Kinetic plot for the RAFT polymerization of NIPAM with the [G-3]-based RAFT agent at 80 °C and (b) evolution of the molecular weights and polydispersities with the conversion during polymerization.

merization of NIPAM or the RAFT copolymerization of NIPAM and PyBA. The elution peak of the [G-3]-based RAFT agent is symmetric with a narrow polydispersity (M_w/M_n) of 1.02. The elution peaks of [G-3]-PNIPAM and [G-3]-PNIPAM-Py are also symmetric and show no tailing at the lower molecular weight side, indicating a complete consumption of the [G-3]-based RAFT agent. The polydispersities of [G-3]-PNIPAM$_{220}$ and [G-3]-PNIPAM$_{250}$-Py were determined by GPC to be 1.16 and 1.20, respectively. The relatively narrow polydispersities of the dendritic–linear diblock copolymers also support the controlled RAFT polymerization of NIPAM with the [G-3]-based RAFT agent.

For comparison, we also synthesized [G-2]-PNIPAM; the DP of the PNIPAM block was determined to be 235 by ^{1}H NMR, and the polydispersity of [G-2]-PNIPAM$_{235}$ was 1.17, as determined by GPC.

cmc

The dendritic–linear diblock copolymer consisted of a hydrophilic linear PNIPAM block and a hydrophobic [G-2] or [G-3] dendron; this provided an opportunity for these polymers to disperse in the aqueous phase to form supramolecular micellar aggregates. The amphiphilic characteristics of the diblock copolymer were then studied by TEM, LLS, optical transmittance, and fluorescence techniques. All these studies should be carried above the cmc of [G-2]-PNIPAM$_{235}$ or [G-3]-PNIPAM$_{220}$ aqueous solutions. Therefore, it was necessary to measure the cmc first.

Figure 4(a) shows the surface tensions of aqueous solutions of [G-2]-PNIPAM$_{235}$ and [G-3]-PNIPAM$_{220}$ at different concentrations. From the inflection point of the two curves, the cmc values of [G-2]-PNIPAM$_{235}$ and [G-3]-PNIPAM$_{220}$ aqueous solutions were determined to be 1.0×10^{-5} and 6.3×10^{-6} g/mL, respectively. This indicates that the [G-3] dendron is more hydrophobic than the [G-2] dendron; this result is expected because of the chemical geometry of [G-2] and [G-3].

The cmc of [G-3]-PNIPAM$_{220}$ in an aqueous solution can also be determined by a fluorescence technique with pyrene as a probe. Changes in the pyrene fluorescence characteristics are frequently used to monitor the onset of micellization for various amphiphilic block copolymers. The characteristic feature of the pyrene excitation spectra, the

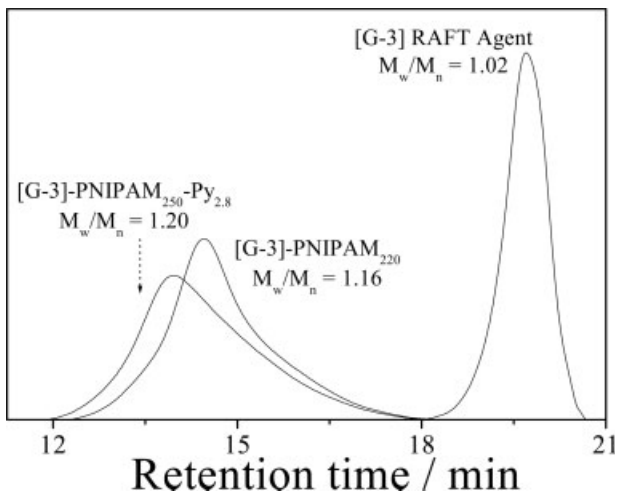

Figure 3. GPC traces of [G-3]-based RAFT agent [G-3]-PNIPAM$_{220}$ and pyrene-labeled [G-3]-PNIPAM$_{250}$-Py$_{2.8}$.

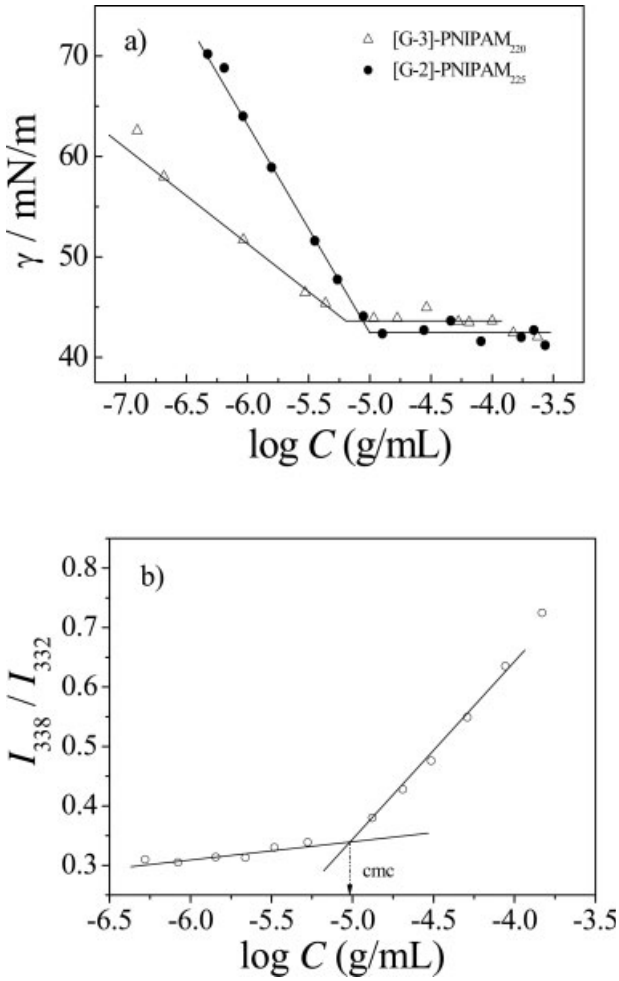

Figure 4. (a) Surface tension versus the concentration of [G-2]-PNIPAM$_{235}$ and [G-3]-PNIPAM$_{220}$ at 20 °C (b) plot of I_{338}/I_{332} from pyrene excitation spectra as a function of the concentration of [G-3]-PNIPAM$_{220}$ in water at. 20 °C. The pyrene concentration was fixed at 5.0×10^{-7} mol/L.

pyrene low-energy (0,0) band, which undergoes a shift from 332 to 338 nm upon pyrene partition into a micellar hydrophobic core, was employed to determine the cmc of dendritic–linear diblock copolymers in water.[11] Figure 4(b) shows the concentration dependence of the intensity ratios (I_{338}/I_{332}) of pyrene excitation spectra in the presence of [G-3]-PNIPAM$_{220}$. At a lower concentration range, a negligible change in I_{338}/I_{332} was detected. However, above a certain concentration, the intensity ratios exhibited a dramatic increase, suggesting that pyrene molecules are incorporated into the hydrophobic core region above the cmc. Therefore, the cmc were determined from the crossover point at the low concentration range in Figure 4(b). The cmc value of [G-3]-PNIPAM$_{220}$ was 9.5×10^{-6} g/mL, which is comparable to that determined by surface tensiometry (6.3×10^{-6} g/mL).

At the cmc, the molar concentration of dendritic–linear diblock copolymer chains is about 3.6×10^{-7} mol/L, which is comparable to the pyrene concentration of 5.0×10^{-7} mol/L; there are about 1.4 pyrene molecules per [G-3]-PNIPAM chain. I_{338}/I_{332} increases markedly only above the cmc, and this hints that pyrene molecules are mainly located inside the void space between [G-3] dendrons but not inside the internal voids of each monodendron; otherwise, the ratio I_{338}/I_{332} would not change considerably above the cmc because the number-density of dendritic–linear diblock copolymer chains is in excess of that of pyrene probes at concentrations above 9.5×10^{-6}. These results also show that the aggregates assembled from [G-3]-PNIPAM can encapsulate hydrophobic guest molecules inside their hydrophobic core.

TEM Characterization

Figure 5 gives typical TEM images of micelles formed from [G-3]-PNIPAM$_{220}$ in water. The aggregates formed in aqueous solutions are spherical and are quite narrowly distributed, ranging from 40 to 80 nm in diameter. Because the dendron size for generation 3.0 is about 1.5–2.0 nm[1] and it takes a relatively dense packing conformation in comparison with the PNIPAM block, it is reasonable to expect that [G-3]-PNIPAM will self-assemble into micelles with aggregated [G-3] as the hydrophobic interior stabilized by a soluble PNIPAM corona.[19] Because of poor packing efficiencies of ball–chain-like units, it is reasonable to speculate that the hydrophobic core consists of loosely aggregated [G-3] dendrons. Because of the molecular size of the [G-3] dendron (1.5–2.0 nm) and the micellar diameter determined by TEM (40–80 nm), which should reflect the dimension of the hydrophobic core, some PNIPAM blocks must be buried inside the hydrophobic core.

Dynamic LLS of the aqueous [G-3]-PNIPAM$_{220}$ solution at 25 °C reveals micellar diameters ranging from 50 to 200 nm, with an average hydrodynamic diameter ($\langle D_h \rangle$) of about 110 nm. It is well known that diameters measured by TEM are typically much smaller than those measured by dynamic LLS because the former reflects conformations in the dry state, whereas $\langle D_h \rangle$ determined by dynamic LLS reflects the dimensions of both the core and the stretched PNIPAM shell. $\langle D_h \rangle$ of [G-3]-PNIPAM$_{220}$ with a fully collapsed PNIPAM shell at 32 °C is about 70 nm (as

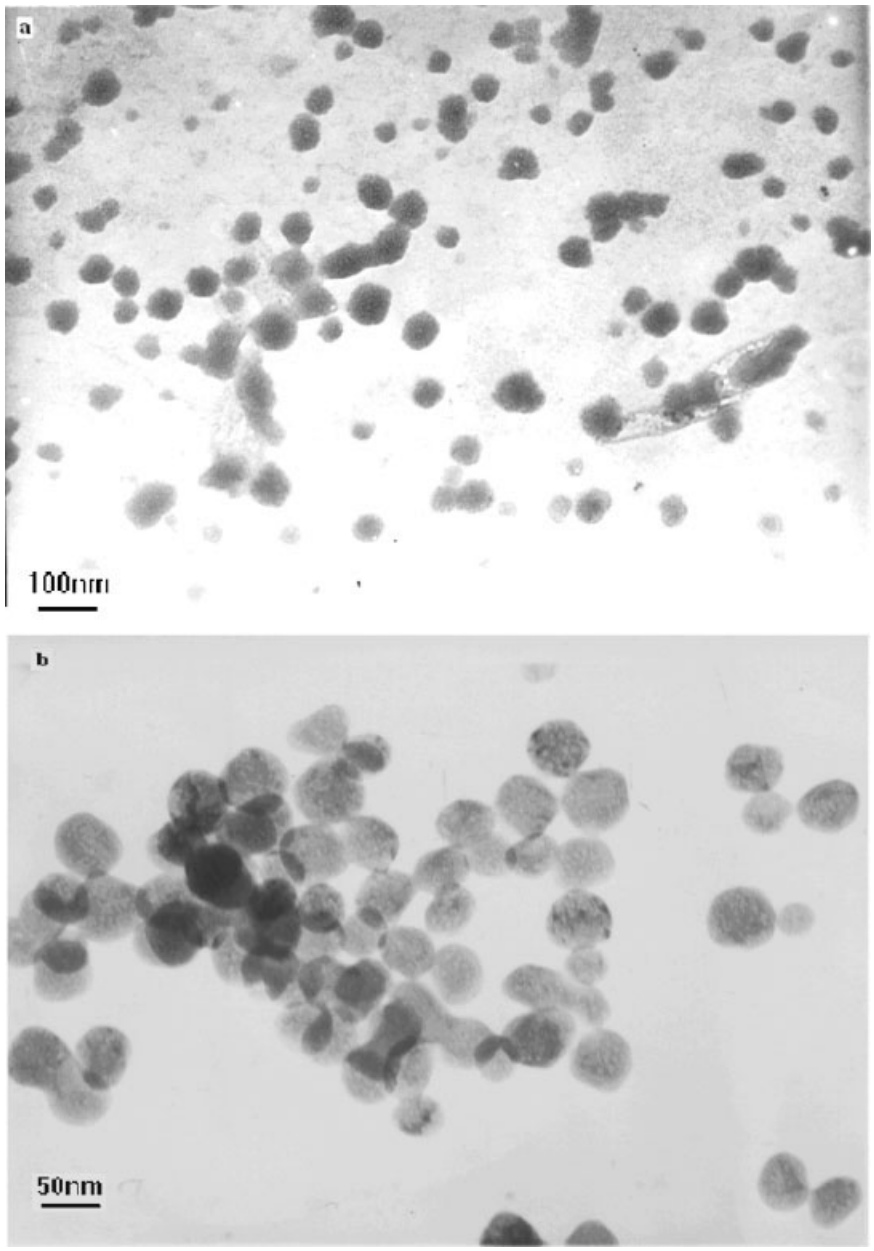

Figure 5. Typical TEM images at two different magnifications. The micelles were assembled from [G-3]-PNIPAM$_{220}$ in water at 25 °C.

described later). The general agreement between sizes measured by dynamic LLS and TEM suggests that the spherical morphologies observed by TEM are present in solution; they are not due to artifacts of substrate adsorption or formed during the solvent-evaporating process.

LLS Characterization

LLS was then used to characterize the chain conformational changes of [G-3]-PNIPAM$_{220}$ upon heating or cooling. It is well known that the PNIPAM homopolymer undergoes a coil–globule phase transition in dilute aqueous solutions at its LCST of about 32 °C.[35] After micellization, [G-3]-PNIPAM$_{220}$ forms core–shell nanostructures with aggregated [G-3] dendrons as the hydrophobic core and soluble PNIPAM as the stabilizing shell. The formed core–shell aggregates should be thermoresponsive because PNIPAM chains are located at the shell. Dynamic and static LLS was used to characterize the sizes and size distributions

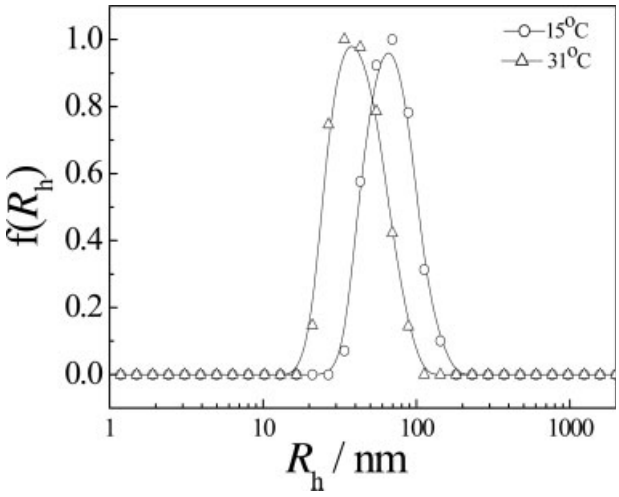

Figure 6. $f(R_h)$ of [G-3]-PNIPAM$_{220}$ micelles at different temperature (15 and 31 °C). The copolymer concentration was 5.0×10^{-5} g/mL.

of the formed aggregates with nanoporous interiors.

Figure 6 shows the hydrodynamic radius distribution [$f(R_h)$] of [G-3]-PNIPAM$_{220}$ at different temperatures (15 and 31 °C). In terms of the distribution width and peak position, $f(R_h)$ shows that the [G-3]-PNIPAM$_{220}$ used in this study is narrowly distributed. At 15 °C, R_h of the micelles ranges from 34 to 143 nm, with the peak located at 69 nm. Upon the heating of the solution to 31 °C, R_h is in the range of 21–88 nm, with the peak located at 34 nm. This reveals a decrease in the particle size upon heating. This must be due to the collapse of PNIPAM brushes at the corona surrounding the hydrophobic interior composed of [G-3] dendrons. The aggregates are very monodisperse, and the polydispersity indices of the size distributions (μ_2/Γ^2) are typically less than 0.1 over the whole temperature range of 15–32 °C. This is in agreement with the TEM results.

Figure 7 shows the temperature dependence of the apparent molecular weight ($M_{w,app}$) of the nanoparticles. $M_{w,app}$ remains almost constant at about 5.1×10^6 g mol^{-1} in the temperature range of 15–32 °C. Above 32 °C, the nanoparticles slightly aggregate, as evidenced by the dramatic increase in $M_{w,app}$. The molecular weight of [G-3]-PNIPAM$_{220}$ has been calculated to be 2.66×10^4 g mol^{-1}, and the average aggregation number of [G-3]-PNIPAM$_{220}$ chains inside each aggregate below 32 °C is about 190.

TEM images shown in Figure 5 reveal an average core size of about 60 nm. Therefore, the grafting density of PNIPAM chains on the porous core can be calculated. The average surface area per PNIPAM chain is ~60 nm^2. This reflects a very sparse grafting of PNIPAM chains at the surface of the [G-3] core, which must be due to poor packing efficiency because the dendritic–linear diblock copolymer chain takes a ball–chain conformation.[42] This rough calculation will certainly incur large errors because we assume that all PNIPAM chains are located at the corona of the porous core. This is actually not the case because some PNIPAM chains should be located inside the porous micellar interior on account of the large difference between the size of the micellar core and the size of [G-3] monodendrons.

When the temperature was increased from 32 to 37 °C, $M_{w,app}$ of the aggregates increased 6 times, and the average aggregation number per aggregate increased from 190 to 1140. The aggregation is due to the decreased solubility of the PNIPAM chain at the nanoparticle shell above its LCST. To make things simpler, for the LLS studies described later, we concentrate on temperatures below 32 °C to study the temperature-dependent conformational changes of PNIPAM chains to exclude the complexities incurred by intermicellar aggregation.

Figure 8(a) shows the temperature dependence of the average hydrodynamic radius ($\langle R_h \rangle$) and $\langle R_g \rangle$ of the nanoparticles upon heating. Each data point was obtained after the measured values were stable. At increasing temperatures, $\langle R_h \rangle$ decreases monotonically from 63 to 37 nm in the temperature range of 15–31 °C. This corresponds

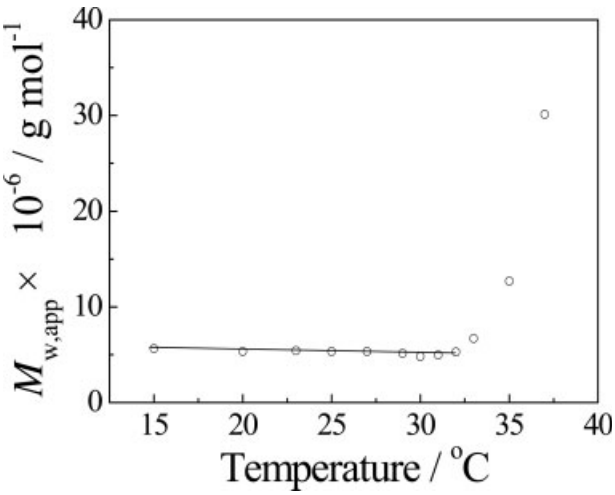

Figure 7. Temperature dependence of $M_{w,app}$ of aggregates formed by [G-3]-PNIPAM$_{220}$ in an aqueous solution. The copolymer concentration was 5.0×10^{-5} g/mL.

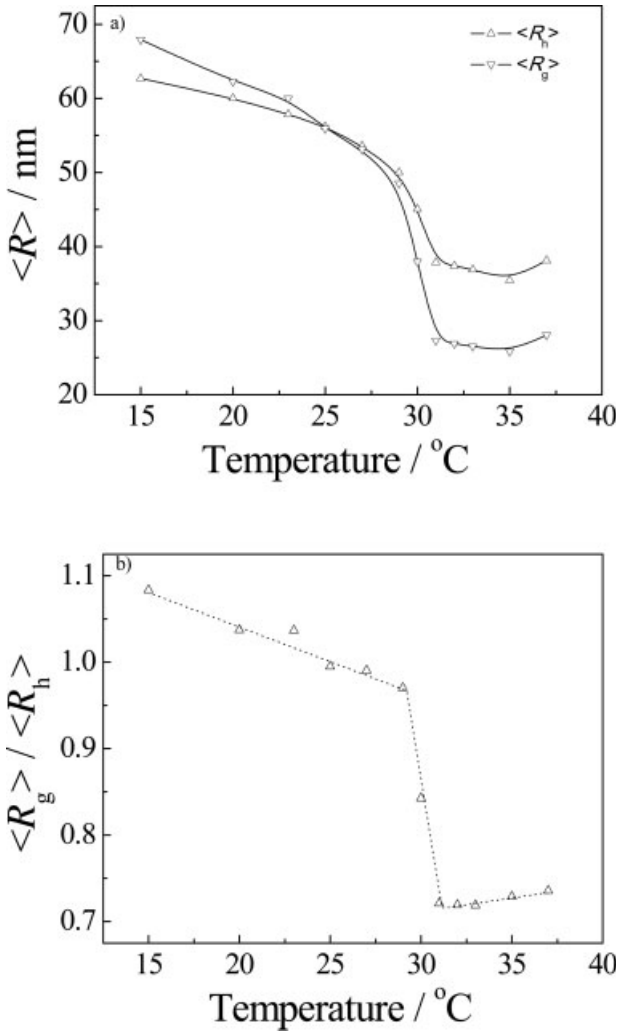

Figure 8. (a) Temperature dependence of $\langle R_g \rangle$ and $\langle R_h \rangle$ and (b) temperature dependence of $\langle R_g \rangle / \langle R_h \rangle$ of [G-3]-PNIPAM$_{220}$ micellar solutions at a concentration of 5.0×10^{-5} g/mL.

to an 80% decrease in the volume of the aggregates. $\langle R_g \rangle$ decreases from 68 to 28 nm in the temperature range of 15–31 °C. A closer check of Figure 8(a) indicates that $\langle R_h \rangle$ and $\langle R_g \rangle$ show the same kind of temperature dependence. In the temperature range of 15–29 °C, $\langle R_h \rangle$ and $\langle R_g \rangle$ exhibit a relatively gradual decrease. The biggest drop in $\langle R_h \rangle$ and $\langle R_g \rangle$ takes place in the narrow temperature range of 29–31 °C, and this should be due to the hydrodynamic collapse of the PNIPAM shell. Our results here are consistent with the coil-to-globule transition of PNIPAM chains attached to PS latex particles.[43]

$\langle R_h \rangle$ drops ~26 nm after the micelles shrink from their swollen state at 15 °C to the fully collapsed state at 31 °C. In preliminary experiments, we found that $\langle R_h \rangle$ of the free PNIPAM homopolymer chain with a DP of 220 is less than 5 nm. This may indicate that PNIPAM chains in the [G-3]-PNIPAM$_{220}$ micelles are stretched. However, because the average surface area per PNIPAM chain is ~60 nm^2, PNIPAM chains at the corona should not stretch to such an extent because the crowding and repulsion between neighboring PNIPAM chains is not expected to be very large. A highly possible explanation is that during the micellization process, [G-3]-PNIPAM$_{220}$ chains first aggregate into small aggregates with relatively low aggregation numbers at low water contents; with further increasing water contents, small aggregates further fuse or merge into larger aggregates stabilized by PNIPAM chains located at the corona. The micellar interior has a lower density of PNIPAM chains than that at the corona. This can also explain why the micellar interior is porous. Upon heating, all PNIPAM chains located inside the interior and at the corona undergo a coil-to-globule transition and collapse. The aggregates thus show a relatively large drop of 26 nm in $\langle R_h \rangle$ upon heating.

We also plotted the temperature dependence of the ratio $\langle R_g \rangle / \langle R_h \rangle$, which reflects the chain density distribution of the dendritic–linear diblock copolymer micelles [Fig. 8(b)]. $\langle R_g \rangle / \langle R_h \rangle$ can reflect the conformation of a polymer or the structure of a particle. For a uniform, nondraining sphere, hyperbranched cluster, and random coil, $\langle R_g \rangle / \langle R_h \rangle$ is ~0.774, 1.0–1.2, and 1.5–1.8, respectively.[44–46] At lower temperatures (<20 °C), $\langle R_g \rangle / \langle R_h \rangle$ is about 1.1; this is the typical $\langle R_g \rangle / \langle R_h \rangle$ value observed for hairy core–shell nanoparticles and indicates that [G-3]-PNIPAM$_{220}$ chains form relatively uniform and slightly draining spherical micelles. $\langle R_g \rangle / \langle R_h \rangle$ decreases from 1.1 to 0.97 in the range of 20–29 °C. In the temperature range of 29–31 °C, $\langle R_g \rangle / \langle R_h \rangle$ decreases sharply from 0.97 to 0.72. At 31 °C, $\langle R_g \rangle / \langle R_h \rangle$ exhibits a small minimum (~0.72); the micelles are now expected to take a nondraining, hard-sphere conformation because of the fully collapsed state of PNIPAM chains.

Therefore, it is evident from LLS results that for PNIPAM chains anchored from a hydrophobic core composed of [G-3] dendrons, their thermoresponsive collapse is a two-stage process. The first one occurs gradually in a broad temperature range (15–29 °C), which is much lower than the LCST of linear PNIPAM homopolymers (ca. 32 °C), followed by the second process, in which the main collapse of PNIPAM chains takes place

in the narrow temperature range of 29–31 °C. It is well known that the LCST of PNIPAM can be finely tuned when it is randomly copolymerized or block-copolymerized with a hydrophilic or hydrophobic monomer, which will accordingly increase or decrease the LCST. The two-stage collapse process is possibly due to the fact that PNIPAM chains are covalently linked to a hydrophobic interior composed of [G-3] dendrons; PNIPAM segments neighboring the hydrophobic interior will behave differently than that located at the outer part of the corona. Zhu et al. and Tenhu et al. reported that PNIPAM chains grafted onto PS latex particles or gold nanoparticles show wider phase-transition ranges or even two well-separated phase transitions.[42,43,47,48] The LLS results observed here seem to agree with the aforementioned experimental results.

Upon the heating of micellar solutions of [G-2]-PNIPAM$_{235}$, similar results are obtained. $\langle R_h \rangle$ of a [G-2]-PNIPAM$_{235}$ micellar solution is 41 nm at 20 °C, which is smaller than that of [G-3]-PNIPAM$_{220}$; this is expected because the molecular size of the [G-3] dendrimer is larger than that of [G-2]. $\langle R_h \rangle$ decreases to 29 nm at 31 °C. Above 31 °C, intermicellar aggregation takes place.

This temperature-dependent collapse of dendritic–linear diblock copolymer micelles is worth further exploitation. At lower temperatures, PNIPAM chains at the corona are in an extended conformation, and there exist pores for guest molecules to diffuse into the hydrophobic and nanoporous interior. At higher temperatures, the pores are closed because of the collapse of PNIPAM chains, and the whole aggregates exist as densely packed spheres. In comparison with diblock copolymer micelles, one of the advantages is that the hydrophobic interior of dendritic–linear diblock copolymer micelles is not entangled. If the size of the guest molecule is appropriate, the diffusion both in and out of the dendritic–linear diblock copolymer micelles should be quite quick; most importantly, temperature variation can be used to finely tune the diffusion rate.

Optical Transmittance

Figure 9 shows the temperature dependence of transmittance at 500 nm for micelles prepared from [G-3]-PNIPAM$_{220}$. A much higher concentration (5.0×10^{-4} g/mL) compared to that for light scattering studies was used here to have enough detection sensitivity. Figure 9 shows that at about 30 °C, the transmittance starts to decrease dramatically. The decrease of the transmittance should be correlated with the increase of the scattering light intensity. Therefore, the decrease in transmittance above 30 °C should be due to the aggregation of micelles with collapsed PNIPAM shells. Micelles with already collapsed PNIPAM brushes tend to collide with each other at the concentration studied; this kind of collision will surely contribute to intermicellar aggregation because the PNIPAM corona becomes sticky above their LCST.[49] The transmittance decreases from 100% at room temperature to 40–50% at 40 °C, and then stabilizes at even higher temperatures. There is no macroscopic phase separation after storage at 50 °C for 12 h. The temperature dependence of the transmittance of [G-2]-PNIPAM$_{235}$ gives similar result (data not shown); the phase-transition temperature is also around 30 °C.

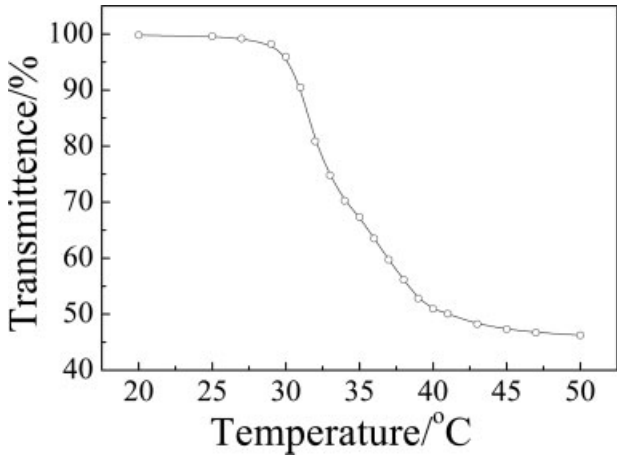

Figure 9. Temperature dependence of the transmittance of an aqueous solution of [G-3]-PNIPAM$_{220}$. The copolymer concentration was 8.0×10^{-4} g/mL.

Fluorescence Measurements

Pyrene has been widely used as a probe of structure and dynamics in macromolecular systems because of its long excited-state lifetime and spectral sensitivity to the surrounding medium. Excimer fluorescence measured by the excimer-to-monomer ratio (I_e/I_m) provides highly localized information because the excimer is only formed when aromatic rings closely approach each other within 4–5 Å.[50–52] Here we selectively labeled the PNIPAM block of [G-3]-PNIPAM dendritic–linear block amphiphiles with pyrene (we denote it [G-3]-PNIPAM-Py). The pyrene content determined by UV–vis absorption with 1-pyrenebutanol as a

model compound is 1.1 mol % on the basis of the NIPAM units; on average, there are 2.8 pyrene units per PNIPAM block with a DP of 250. The fluorescence spectra of aqueous solutions of [G-3]-PNIPAM$_{250}$-Py$_{2.8}$ at different temperatures are shown in Figure 10. Besides the monomer bands that are characteristic of the pyrene vibronic structure, which exhibits three distinct peaks at 373, 393, and 415 nm, the excimer emission of pyrene appears as a broad, structureless band around 480 nm. The spectral parameter of interest to us is the excimer (ca. 480 nm)-to-monomer (373 nm) intensity ratio (I_e/I_m).

Figure 11 depicts the temperature dependence of I_e/I_m for aqueous solutions of [G-3]-PNIPAM$_{250}$-Py$_{2.8}$. The typical measuring accuracy of I_e/I_m is ± 0.01 in the whole temperature range studied. On average, there are 2.8 pyrene groups per PNIPAM chain. Excimer fluorescence can originate from the contact of pyrene groups from the same or different PNIPAM chains located at the corona. I_e/I_m first gradually increases in the range of 15–20 °C, reaches a maximum at 20 °C, and then decreases in the temperature range of 20–32 °C. Although we observe by LLS that, in the temperature range of 15–29 °C, both $\langle R_g \rangle$ and $\langle R_h \rangle$ exhibit a gradual decrease, the different trends of I_e/I_m below and above 20 °C tell us that below 20 °C, the decrease of $\langle R_g \rangle$ and $\langle R_h \rangle$ is due to solvent worsening, water is starting to become

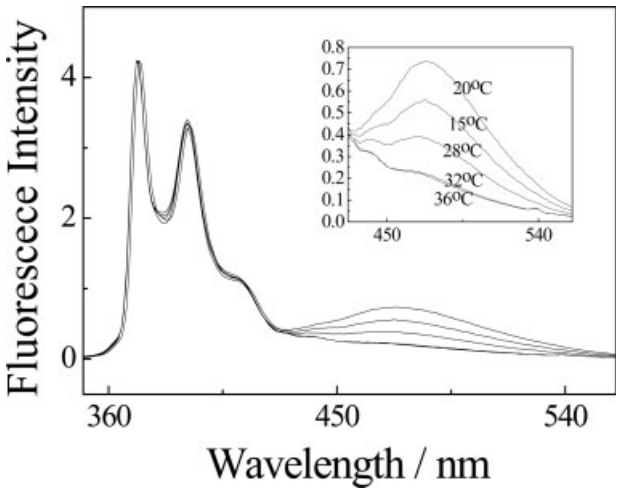

Figure 10. Fluorescence emission spectra for [G-3]-PNIPAM$_{250}$-Py$_{2.8}$ in water at different temperatures. The spectra are normalized with respect to the monomer emission at 373 nm. The inset shows an enlarged portion of the pyrene excimer emission spectra at different temperatures (20, 15, 28, 32, and 36 °C from top to bottom).

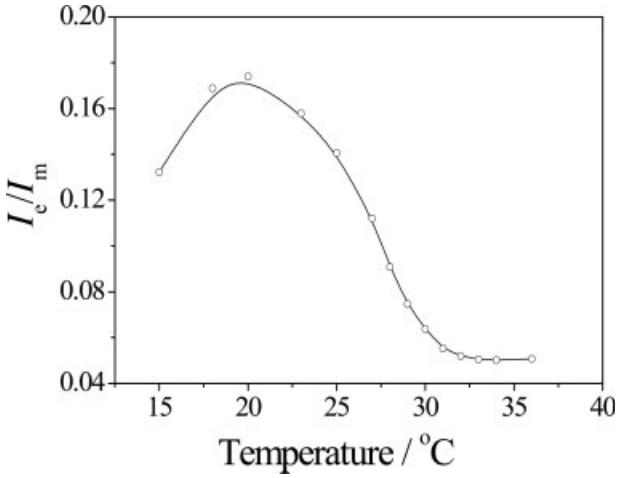

Figure 11. Ratio of the pyrene excimer emission intensity at 480 nm to the pyrene monomer emission intensity at 373 nm (I_e/I_m) of [G-3]-PNIPAM$_{250}$-Py$_{2.8}$ in water as a function of temperature. The copolymer concentration was 2.0×10^{-4} g/mL. The excitation wavelength was 330 nm.

a poor solvent, and the PNIPAM chain still remains in a random coil conformation in this temperature range;[53] in the broad temperature range of 20–32 °C, the collapse of the PNIPAM chain takes place. The continuous decrease of I_e/I_m should be due to the collapse of the PNIPAM chain; it is getting more hydrophobic, the mobility of chains as well as linked chromophores are increasingly restrained, and they get fewer chances to come close to one another. From excimer fluorescence results, we can tell that PNIPAM chains indeed start to collapse at 20 °C, but this does not support the idea that the collapse of the PNIPAM chain is a two-stage process in the temperature range of 20–31 °C. This is due to the fact that pyrene groups are randomly distributed on PNIPAM chains; it cannot differentiate collapsing processes taking place in the inner and outer parts of the PNIPAM shell. The conclusion of two-stage collapse from LLS results should still hold.

CONCLUSIONS

A poly(benzyl ether)–poly(*N*-isopropylacrylamide) dendritic–linear diblock copolymer was prepared by the RAFT polymerization of NIPAM in 1,4-dioxane with a third-generation-dendrimer-based RAFT agent. Studies of the polymerization kinetics indicated a controlled living free-radical polymerization process. In an aqueous solution, amphiphilic [G-3]-PNIPAM self-assembled into micelles

with a hydrophobic core composed of aggregated [G-3] and a thermoresponsive PNIPAM shell. By a combination of LLS and excimer fluorescence, we determined that for PNIPAM chains sparsely anchored from a porous core composed of [G-3] dendrons, their thermoresponsive collapse was a two-stage process. The first one occurred gradually in the temperature range of 20–29 °C, which was much lower than the LCST of the linear PNIPAM homopolymer, and it was followed by the second process, in which the main collapse of PNIPAM chains took place in the narrow temperature range of 29–31 °C.

This work was supported by an Outstanding Youth Fund (50425310) and a Key Research Grant (20534020) from the National Natural Scientific Foundation of China and by the Bai Ren Project of the Chinese Academy of Sciences.

REFERENCES AND NOTES

1. (a) Tomalia, D. A.; Durst, H. D. Top Curr Chem 1993, 165, 193; (b) Fréchet, J. M. J.; Tomalia, D. A. Dendrimers and Other Dendritic Polymers; Wiley: New York, 2001; (c) Newkome, G. R.; Moorrefield, C. N.; Vögtle, F. Dendrimers and Dendrons: Concepts, Syntheses, Applications; Wiley-VCH: Weinheim, 2001.
2. (a) Tomalia, D. A.; Berry, V.; Hall, M.; Hedstrand, D. M. Macromolecules 1987, 20, 1164; (b) Hawker, C. J. Adv Polym Sci 1993, 147, 113; (c) Hawker, C. J.; Wooley, K. L. Science 2005, 309, 1200; (d) Gitsov, I.; Lambrych, K. R. In: Syntheses and Applications in Microspheres, Microcapsules & Liposomes; Arshady, R., Ed.; Citus Books: London, 2002; Vol. 5, p 31.
3. Hawker, C. J.; Wooley, K. L.; Frechét, J. M. J. J Chem Soc Perkin Trans 1993, 1, 1287.
4. (a) Niwa, M.; Higashizaki, T.; Higashi, N. Tetrahedron 2003, 59, 4011; (b) Gitsov, I.; Lin, C. Curr Org Chem 2005, 9, 1025.
5. Haba, Y.; Harada, A.; Takagishi, T.; Kono, K. J Am Chem Soc 2004, 126, 12760.
6. Kimura, M.; Kato, M.; Muto, T.; Hanabusa, K.; Shirai, H. Macromolecules 2000, 33, 1117.
7. You, Y. Z.; Hong, C. Y.; Pan, C. Y.; Wang, P. H. Adv Mater 2004, 16, 1953.
8. (a) Riess, G. Prog Polym Sci 2003, 28, 1107; (b) Zhu, C.; Hard, C.; Lin, C. P.; Gitsov, I. J Polym Sci Part A: Polym Chem 2005, 43, 4017; (c) Vestberg, R.; Nilsson, C.; Lopes, C.; Lind, P.; Eliasson, B.; Malmstrm, E. J Polym Sci Part A: Polym Chem 2005, 43, 1177; (d) Lee, C. C.; Grayson, S. M.; Fréchet, J. M. J. J Polym Sci Part A: Polym Chem 2004, 42, 3563.
9. Gil, E. S.; Hudson, S. A. Prog Polym Sci 2004, 29, 1173.
10. Liu, S.; Weaver, J. V. M.; Tang, Y.; Billingham, N. C.; Armes, S. P.; Tribe, K. Macromolecules 2002, 35, 6121.
11. (a) Gitsov, I.; Lambrych, K. R.; Remnant, V. A.; Pracitto, R. J Polym Sci Part A: Polym Chem 2000, 38, 2711; (b) Gitsov, I. InAdvances in Dendritic Macromolecules; Newkome, G. R., Ed.; Elsevier Science: Amsterdam, 2002; Vol. 5, pp 45–87.
12. (a) Lambrych, K. R.; Gitsov, I. Macromolecules 2003, 36, 1068; (b) Santini, C. M. B.; Johnson, M. A.; Boedicker, J. Q.; Hatton, T. A.; Hammond, P. T. J Polym Sci Part A: Polym Chem 2004, 42, 2784.
13. Gillies, E. R.; Jonsson, T. B.; Fréchet, J. M. J. J Am Chem Soc 2004, 126, 11936.
14. Gitsov, I.; Fréchet, J. M. J. J Am Chem Soc 1996, 118, 3785.
15. (a) Leduc, M. R.; Hawker, C. J.; Dao, J.; Fréchet, J. M. J. J Am Chem Soc 1996, 118, 11111; (b) Sill, K.; Emrick, T. J Polym Sci Part A: Polym Chem 2005, 43, 5429.
16. Leduc, M. R.; Hayes, W.; Fréchet, J. M. J. J Polym Sci Part A: Polym Chem 1998, 36, 1.
17. (a) Gitsov, I.; Wooley, K. L.; Hawker, C. J.; Ivanova, P. T.; Frechet, J. M. J. Macromolecules 1993, 26, 5621; (b) Namazi, H.; Adeli, M. J Polym Sci Part A: Polym Chem 2005, 43, 28.
18. Gitsov, I.; Wooley, K. L.; Fréchet, J. M. J. Angew Chem Int Ed Engl 1992, 31, 1200.
19. Gitsov, I.; Frechet, J. M. J. Macromolecules 1993, 26, 6536.
20. van Hest, J. C. M.; Baars, M. W. P.; Elissen-Román, C.; van Genderen, M. H. P.; Meijer, E. W. Macromolecules 1995, 28, 6689.
21. van Hest, J. C. M.; Delnoye, D. A. P.; Baars, M. W. P. L.; Elissen-Roman, C.; van Genderen, M. H. P.; Meijer, E. W. Chem—Eur J 1996, 2, 1616.
22. Chapman, T. M.; Hillyer, G. L.; Mahan, E. J.; Shaffer, K. A. J Am Chem Soc 1994, 116, 11195.
23. Gitsov, I.; Ivanova, P. T.; Fréchet, J. M. J. Macromol Rapid Commun 1994, 15, 387.
24. (a) Zhu, L. Y.; Tong, X. F.; Li, M. Z.; Wang, E. J. J Polym Sci Part A: Polym Chem 2000, 38, 4282; (b) Zhu, L. Y.; Zhu, G. L.; Li, M. Z.; Wang, E. J.; Zhu, R. P.; Qi, X. Eur Polym J 2002, 38, 2503.
25. Chiefari, J.; Chong, Y. K.; Ercole, F.; Krstina, J.; Le, T. P. T.; Mayadunne, R. T. A.; Meijs, G. F.; Moad, G.; Moad, C. L.; Rizzardo, E.; Thang, S. H. Macromolecules 1998, 31, 5559.
26. Chiefari, J.; Moad, G.; Rizzardo, E.; Gridnev, A. A. (E. I. du Pont de Nemours and Co. and Commonwealth Scientific and Industrial Research Organization). U.S. Patent 9,847,927, 1998.
27. Rizzardo, E.; Chiefari, J.; Mayadunne, R. T. A.; Moad, G.; Thang, S. H. ACS Symp Ser 2000, 768, 278.
28. Cölfen, H. Macromol Rapid Commun 2001, 22, 219.

29. Gohy, J. F.; Lohmeijer, B. G. G.; Varshney, S. K. Macromolecules 2002, 35, 9748.
30. Hadjikallis, G.; Hadiyannakou, S. C.; Vamvakaki, M. Polymer 2002, 43, 7269.
31. Andre, X.; Zhang, M. F.; Muller, A. H. E. Macromol Rapid Commun 2005, 26, 558.
32. Rodriguez-Hernandez, J.; Lecommandoux, S. J Am Chem Soc 2005, 127, 2026–2027.
33. Arotcarena, M.; Heise, B.; Ishaya, S.; Laschewsky, A. J Am Chem Soc 2002, 124, 3787.
34. Save, M.; Weaver, J. V. M.; Armes, S. P.; McKenna, P. Macromolecules 2002, 35, 1152.
35. Schild, H. G. Prog Polym Sci 1992, 17, 163.
36. Ganachaud, F.; Monteiro, M. J.; Gilbert, R. G.; Dourges, M.-A.; Thang, S. H.; Rizzardo, E. Macromolecules 2000, 33, 6738.
37. Schilli, C.; Lanzendörfer, M. G.; Müller, A. H. E. Macromolecules 2002, 35, 6819.
38. Favier, A.; Charreyre, M.-T.; Chaumont, P.; Pichot, C. Macromolecules 2002, 35, 8271.
39. (a) Ray, B.; Isobe, Y.; Morioka, K.; Habaue, S.; Okamoto, Y.; Kamigaito, M.; Sawamoto, M. Macromolecules 2003, 36, 543; (b) Perrier, S.; Takolpuckdee, P. J Polym Sci Part A: Polym Chem 2005, 43, 5347; (c) Liu, B.; Perrier, S. J Polym Sci Part A: Polym Chem 2005, 43, 3643; (d) Monteiro, M. J. J Polym Sci Part A: Polym Chem 2005, 43, 3189.
40. (a) Convertine, A. J.; Ayres, N.; Scales, C. W.; Lowe, A. B.; McCormick, C. L. Biomacromolecules 2004, 5, 1177; (b) Savariar, E. N.; Thayumanavan, S. S. J Polym Sci Part A: Polym Chem 2004, 42, 6340; (c) Hong, C. Y.; You, Y. Z.; Pan, C. Y. J Polym Sci Part A: Polym Chem 2004, 42, 4873; (d) Drockenmuller, E.; Li, L. Y. T.; Harth, E.; Russell, T. P.; Kim, H. C.; Hawker, C. J. J Polym Sci Part A: Polym Chem 2005, 43, 1028.
41. Hawker, C. J.; Frechet, J. M. J. J Am Chem Soc 1990, 112, 7638.
42. Halperin, A.; Tirrell, M.; Lodge, T. P. Adv Polym Sci 1992, 100, 31.
43. Zhu, P. W.; Napper, D. H. J Colloid Interface Sci 1994, 164, 489.
44. Burchard, W. InLight Scattering Principles and Development; Brown, W., Ed.; Clarendon: Oxford, 1996; p 439.
45. Burchard, J. P.; Roovers, J.; Freed, K. F. Macromolecules 1990, 23, 418.
46. Douglas, J. P.; Roovers, J.; Freed, K. F. Macromolecules 1990, 23, 418.
47. Zhao, B.; Brittain, W. J. Prog Polym Sci 2000, 25, 677.
48. Shan, J.; Chen, J.; Nuopponen, M.; Tenhu, H. Langmuir 2004, 20, 4671.
49. Zhang, W. A.; Zhou, X. C.; Li, H.; Fang, Y. E.; Zhang, G. Z. Macromolecules 2005, 38, 909.
50. Chen, W.; Durning, C. J.; Turro, N. J. Macromolecules 1999, 32, 4151.
51. Kalyanasundaram, K.; Thomas, J. K. J Am Chem Soc 1977, 99, 2039.
52. Winnik, F. M. Macromolecules 1990, 23, 233.
53. Picarra, S.; Duhamel, J.; Fedorov, D. A.; Martinho, J. M. G. J Phys Chem B 2004, 108, 12009.